PAPER

Human stem cell response to layered zirconium phosphate

Jin Nakamura, [ID] *[ab] Kanta Endo,[b] Ayae Sugawara-Narutaki [ID] [c] and Chikara Ohtsuki [ID] *[b]

This study aims to evaluate the *in vitro* cytocompatibility of layered zirconium phosphate (ZP) and its derivative material that was organically modified using glycerophosphate (ZGP). The ZP and ZGP particles were prepared *via* a reflux method in an aqueous solution containing phosphoric acid. The field emission scanning electron microscopy showed the prepared samples were fine particles with 70–100 nm diameter. X-ray diffraction and Raman spectrometry indicated the presence of a layered crystal structure. The interlayer distance of ZP was estimated to be 0.76 nm from the 002 diffraction. Modification of ZP with β-glycerophosphate, lead to expansion of the interlayer distance of 0.85 nm. Grazing incidence X-ray diffraction and Raman spectrometry showed that the crystal structures of ZP and ZGP were maintained even after the samples were coated onto polyethylene (PE) substrates *via* hot pressing. The water droplet contact angles on the PE substrates coated with the ZP and ZGP particles (ZP/PE and ZGP/PE) were 2 ∼ 6° lesser than that on the uncoated PE substrate. After human adipose-derived stem cells (hASCs) were cultured on the substrates, 2.5–3.5 times higher numbers of adhered cells were observed on the substrates coated with ZP and ZGP than on the uncoated PE substrates and 1.1–1.6 times higher than on the substrate coated with hydroxyapatite particles (HAp/PE). Increasing cell numbers were observed after culturing for 24 h, indicating that the ZP/PE and ZGP/PE showed low cytotoxicity to the hASCs. Furthermore, the ZP/PE showed the highest area of hASC adhesion among all the samples. These results highlight the possibility that layered zirconium phosphate and its organically modified substances can be applied to biomaterials for tissue repair.

1. Introduction

Among ceramic biomaterials, certain substances exhibit biological affinity for human body tissues. These so-called bioactive ceramics can directly bond to living bone after implantation in a bone defect.[1] Hydroxyapatite, a type of calcium phosphate ceramic, is a widely used bioactive ceramic and shows high affinity not only to bone but also soft tissues.[2,3] Thus, hydroxyapatite has been studied for use as a bone repair material, percutaneous terminal, and coating material on catheter surfaces.[4–6] In recent years, the development of bioactive ceramics with high functionality has aimed to facilitate multifunctionality such as enhancement of tissue regeneration and antibacterial action.[7–9] Although surface modification of ceramics has been attempted to incorporate organic molecules and inorganic ions as biological factors to enhance bone-

formation or facilitate antibacterial properties, it has been difficult to derive satisfactory physiological functions from conventional bioactive ceramic materials.[7,10–13] It is therefore worth developing novel biomaterials capable of controlled release of biological factors as well as high biological affinity.

Inorganic materials with layered structure have received much attention for controlled dissolution through organic modification of their interlayers. Various inorganic layered compounds, namely, clays,[14,15] layered double hydroxides,[16] and layered phosphate,[17,18] have been explored as drug delivery carriers and gene reservoirs. Among the layered compounds, the authors pay attention to alpha-zirconium phosphate (α-ZrP: $Zr(HPO_4)_2 \cdot H_2O$) because it is composed of popular inorganic substances—zirconia and phosphate. α-ZrP has a layered crystal structure that allows for incorporation of inorganic ions *via* ion-exchange as well as the capability for organic modification of the interlayers.[19–21] However, there has been little research into the biological affinity of zirconium phosphate. In the present study, we investigated the synthesis of α-ZrP powder as well as its derivative modified using β-glycerophosphoric acid. These materials were coated on a polyethylene (PE) substrate and examined *in vitro via* culturing of human adipose-derived stem cells (hASCs).

[a]Institute for Advanced Research, Nagoya University, Furo-cho, Chikusa-ku, Nagoya 464-8603, Japan. E-mail: nakamura@chembio.nagoya-u.ac.jp

[b]Department of Materials Chemistry, Graduate School of Engineering, Nagoya University, Furo-cho, Chikusa-ku, Nagoya 464-8603, Japan. E-mail: ohtsuki@chembio.nagoya-u.ac.jp

[c]Department of Energy Engineering, Graduate School of Engineering, Nagoya University, Furo-cho, Chikusa-ku, Nagoya 464-8603, Japan

2. Materials and methods

2.1. Preparation of zirconium phosphate and its organic modification

The preparation procedures were developed through appropriate modification of a previously employed technique for synthesis of α-ZrP under suitable conditions.[22] A total of 5 g of zirconylchloride octahydrate (ZrOCl$_2$·8H$_2$O, Kanto Chemical Co., Inc., Japan) and 18 cm^3 of phosphoric acid solution (85 wt%, H$_3$PO$_4$, Nacalai Tesque Inc., Japan) were mixed in 30 cm^3 of deionized water. The mixture was refluxed at 100 °C for 24 h under stirring. The product was centrifuged at 6500 × g for 10 min (MX-301, Tomy Seiko Co., Ltd., Japan) and then dispersed in ultrapure water (40 cm^3) *via* sonication. The centrifugation and redispersion processes were repeated three times. Subsequently, the sample was dried for 1 day in a drying oven (DO-300, Iuchi, Japan), set at 65 °C, and then pulverized. Hereafter, this sample is denoted as ZP.

For the preparation of the organically modified sample, 0.30 g of ZP and 5.50 g of β-glycerophosphate sodium salt hydrate (β-GP; C$_3$H$_7$O$_6$P·2Na[5H$_2$O], Cayman Chemical Co., USA) were mixed in 90 cm^3 of deionized water. The mixture was refluxed at 70 °C for 48 h under stirring. The product was then washed *via* the same centrifugation and redispersion processes as described above for preparation of ZP. Following this, the washed sample was dried for 1 day at 65 °C. This sample (that is, organically modified ZP) is denoted as ZGP.

Powder X-ray diffraction (XRD) patterns of the samples were obtained using an X-ray diffractometer (RINT-2100/PC, Rigaku Co., Japan) with Cu-Kα radiation. The diffraction peaks of ZGP were indexed by using the method described elsewhere.[23] The model of layered crystalline structure consisting of Zr, P and O atoms was prepared from the dimension along the c^*-axis of organically modified ZrP.[23] The powder diffraction patterns of this model were calculated in the space group $P2_1/c$ with monoclinic angles (β) in the range of 91°–125° with using VESTA software.[24] Once the peak position of calculated pattern was matched with the one of ZGP, the lattice constant was refined by least-squares method using MDI Jade 5.0 software (Materials Data Inc., USA). The samples were evaluated using Fourier-transformed infrared spectroscopy (FT-IR, FT/IR-6100, Jasco Co., Japan), *via* the KBr pellet method, and using Raman spectroscopy (ApaRAMAN-Micro/CZ, Lucir Inc., Japan) equipped with a diode-pumped solid state laser (532 nm, 150 mW). The morphology of the samples was observed under a field emission scanning electron microscope (FE-SEM, JSM-7500F, JEOL Ltd., Japan).

2.2. Preparation of substrate samples for cell culture

Four types of samples were prepared by coating the powder samples on the PE substrate. Hydroxyapatite (HAp) powder (Ca$_{10}$(PO$_4$)$_6$(OH)$_2$, HAP-100, Taihei Chemical Industry Co., Ltd) was used as a typical bioactive ceramic. A total of 0.20 g of ZP, ZGP, or hydroxyapatite powder was dispersed in 20 cm^3 of ethanol *via* sonication. A part of the obtained dispersion (30 mm^3) was spread on one side of a high-density PE disc (diameter 14 mm, PEN-050501, AS ONE Co., Japan) and dried at 25 °C. The dried substrate was then placed in a cylindrical press mould, equipped with a band heater, and hot-pressed at 33 MPa for 30 s at 140 °C. The substrates obtained after hot pressing of ZP, ZGP, or the hydroxyapatite are denoted as ZP/PE, ZGP/PE, and HAp/PE, respectively, while the uncoated PE substrate is denoted as PE. The PE was prepared as a control for the cell culture since it is physiologically inert. The crystalline phase on the substrate surfaces was determined by glazing incident X-ray diffraction (GI-XRD, RINT-2100/PC, Rigaku Co., Japan) with an incident beam angle fixed at $\theta = 0.4°$. The surfaces of the coated substrates were also characterized *via* Raman spectroscopy and FE-SEM. The surface roughness of the prepared substrates was evaluated as the arithmetic average roughness using a laser scanning microscope (VK-X1000, Keyence Co., Japan). Ten profile curves were measured for each sample to determine the average roughness (R_a). The wettability of the specimens' surfaces was evaluated under a water contacting angle of 5 mm^3 of deionized water and an ambient atmosphere using a contact angle meter (IMC-159F, Imoto Machinery Co., Ltd., Japan). Image analysis software (ImageJ, National Institute of Health, U.S.A., DropSnake plugin, Ecole Polytechnique Federale de Lausanne, Switzerland) was used for measuring the angle.

2.3. *In vitro* evaluation by cell culture

The prepared substrates were fixed on the well-bottom of a 24-well plate using double-sided tape (command™ tab [M size], CM3PM, 3 M Company, Japan) and sterilized *via* irradiation using an ultraviolet (UV) germicidal lamp. Cytocompatibility was investigated *via* culturing of human adipose-derived stem cells (hASC, ASC-F, Zen-Bio, Inc., USA) on the substrates as per the protocol described in the product manual. The cells were incubated in D-MEM/Ham's F-12 (Wako Pure Chemical Industries, Ltd., Japan) supplemented with 10 vol% foetal bovine serum (Sigma-Aldrich Co. LLC, USA), plated into a 75 cm^2 flask, for 2 weeks at 36.5 °C under 5% CO$_2$. The medium was replaced twice a week. Cells were then detached and re-suspended at a density of 4.0 × 10^4 cells per mL in D-MEM/Ham's F-12 supplemented with 10 vol% foetal bovine serum, dexamethasone (Wako Pure Chemical Industries, Ltd., Japan), L-(+)-ascorbic acid (Wako Pure Chemical Industries, Ltd., Japan), and β-glycerophosphate. Five hundred cubic millimetres of this cell suspension (2.0 × 10^4 cells) was applied on each substrate placed in the well plate and incubated at 36.5 °C under 5% CO$_2$ for 1 or 24 h. After these incubation periods, the cultured samples were fixed with 4% of paraformaldehyde solution (Wako Pure Chemical Industries, Ltd., Japan). The cultured samples were then permeabilized with 0.5%-diluted TritonX-100 solution (Wako Pure Chemical Industries, Ltd., Japan) with the PBS. Subsequently, 1% bovine serum albumin solution (Wako Pure Chemical Industries, Ltd., Japan) was used for blocking at room temperature for 1 h. The vinculin was immunostained with the primary antibody (ABfinity™ Rabbit Monoclonal, Life Technologies Co., USA) overnight at 4 °C. Alexa Fluor® 546 goat anti-rabbit IgG (H + L, highly cross absorbed) (Life Technologies Corporation, U.S.A.) was used as
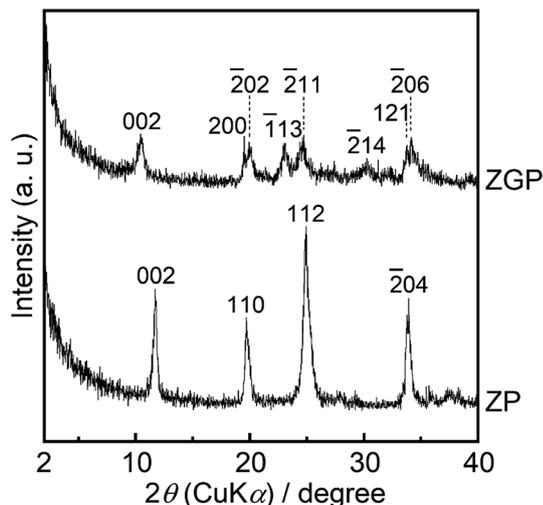
Fig. 1 Powder XRD patterns of the prepared samples.

the secondary antibody. The actin cytoskeleton and nucleus were fluorescently stained with the Alexa Fluor® 488 Phalloidin (Life Technologies Corporation, U.S.A.) and NucBlue™ Fixed Cell Stain ReadyProbes™ reagent (Life Technologies Corporation, U.S.A.), respectively. The samples were rinsed in phosphate buffer saline (PBS, Wako Pure Chemical Industries, Ltd., Japan) before and after the fixation, permeabilization, blocking, and staining procedures. The morphology of adhered cells on the samples was observed using a fluorescence microscope (BZ-X710, Keyence Co., Japan). The numbers of cells were determined via counting of the nuclei in the obtained fluorescent images. The cell-covered areas on substrates were evaluated from the images using image analysis software (BZ-X analyser, Keyence Co., Japan).

3. Results

3.1. Characterization of the prepared powder of ZP and ZGP

Fig. 1 shows powder XRD patterns of the prepared samples of ZP and ZGP. The diffraction pattern of ZP indicated that 002,

110, 112, and $\bar{2}04$ diffractions assigned to α-ZrP were detected according to PDF #33-1482. The diffraction pattern of ZGP sample can be indexed as describing a monoclinic lattice possessing $a = 0.93$ nm, $b = 0.57$ nm, $c = 1.69$ nm and $\beta = 102°$. The peak of 002 diffraction at around $2\theta = 11°$ was shifted to a lower angle than that appearing on the diffraction pattern of ZP. Interlayer distances estimated from the 002 diffraction were approximately 0.76 nm and 0.85 nm for ZP and ZGP, respectively.

Fig. 2(a) shows the FT-IR spectra of the prepared samples of ZP and ZGP. The spectrum of ZP indicates peaks assigned to the P–O asymmetric stretching vibration of the PO_4 group[25] in the region of 1045–1125 cm^{-1} as well as around 970 and 1250 cm^{-1}, which are assigned to in plane bending vibrations of P–O and in plane deformation of P–O–H, respectively.[25–27] The peaks around 3160, 3510, and 3590 cm^{-1} are assigned to water molecules at the interlayer.[26,27] The spectrum of ZGP indicates peaks assigned to the vibrations of the PO_4 group and P–O–C from β-glycerophosphate[28] in the region of 1000–1200 cm^{-1} as
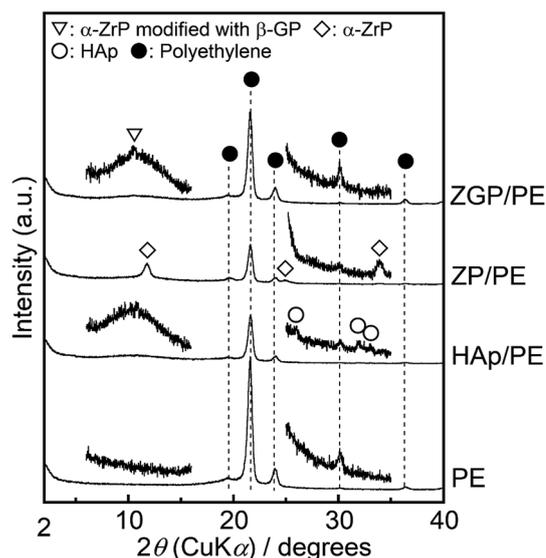

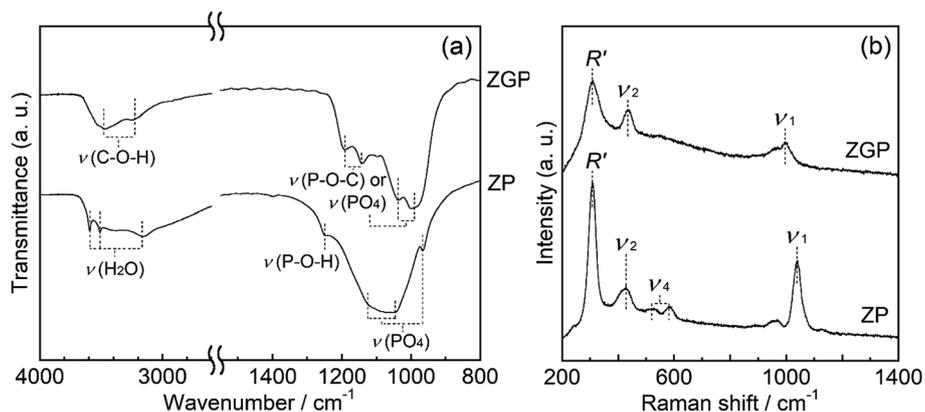Fig. 3 GI-XRD patterns of the prepared substrates.

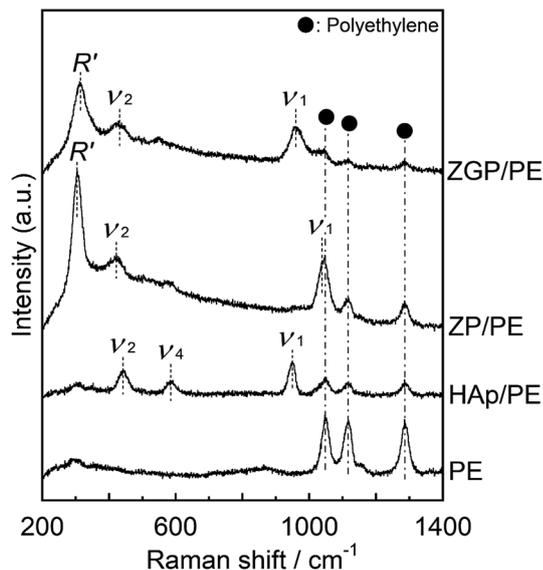Fig. 2 Spectrometric data of the prepared samples. (a) FT-IR spectra, (b) Raman spectra.

Fig. 4 Raman spectra of the prepared substrates.

well as around 3240 and 3470 cm^{-1}, which are assigned to C–O–H stretching vibrations.[28]

The Raman spectra of the prepared samples are shown in Fig. 2(b). ZP shows the spectra that indicated peaks around 1040 cm^{-1}, 580 cm^{-1}, and 430 cm^{-1} originating from internal vibrations of PO$_4$ group, namely symmetric stretching (ν_1), umbrella deformation (ν_4), and asymmetric bending (ν_2) vibration of the PO$_4$ group, respectively.[29] Moreover, the peak

around 310 cm^{-1} is characteristic of a layered structure and is assigned to the external vibration mode (R$'$) involving both Zr atoms and PO$_4$ groups.[29] ZGP showed the peaks of ν_1, ν_2, and R$'$ at 1000, 430, and 310 cm^{-1} respectively. These powder XRD patterns, FT-IR spectra, and Raman spectra support the premise of formation of α-ZrP after the solvothermal processing, and glycerol incorporation in the interlayers in the α-ZrP structure.

3.2. Characterization of the substrates for *in vitro* examination

Fig. 3 shows GI-XRD patterns of the prepared substrates of PE, HAp/PE, ZP/PE, and ZGP/PE. Trace amounts of crystalline phases of α-ZrP (PDF #33-1482), α-ZrP modified with β-GP, and HAp (PDF #09-0432) were detected on the substrate after the coating of ZP, ZGP, and HAp respectively. Fig. 4 shows Raman spectra of the substrates coated with the examined powders. The Raman spectra indicate that PE was present on all the examined substrates. ZP/PE and ZGP/PE showed existence of ZP and ZGP on the substrates by the detection of R$'$, ν_1, and ν_2 vibrations. The Raman spectrum of HAp/PE showed the existence of HAp *via* the detection of ν_1, ν_2, and ν_4 vibrations of the PO$_4$ group[30] at 950, 450, and 580 cm^{-1}, respectively. FE-SEM images of surfaces of the prepared substrates are shown in Fig. 5. The PE substrate appeared to have a smooth surface, while angular-shaped particles of HAp were observed on HAp/PE substrate. ZP/PE and ZGP/PE substrates had aggregations of ZP and ZGP particles, respectively. As shown in the inset of Fig. 5, the prepared samples consisted of fine particles having a diameter of 70–100 nm and aggregation was insignificant.
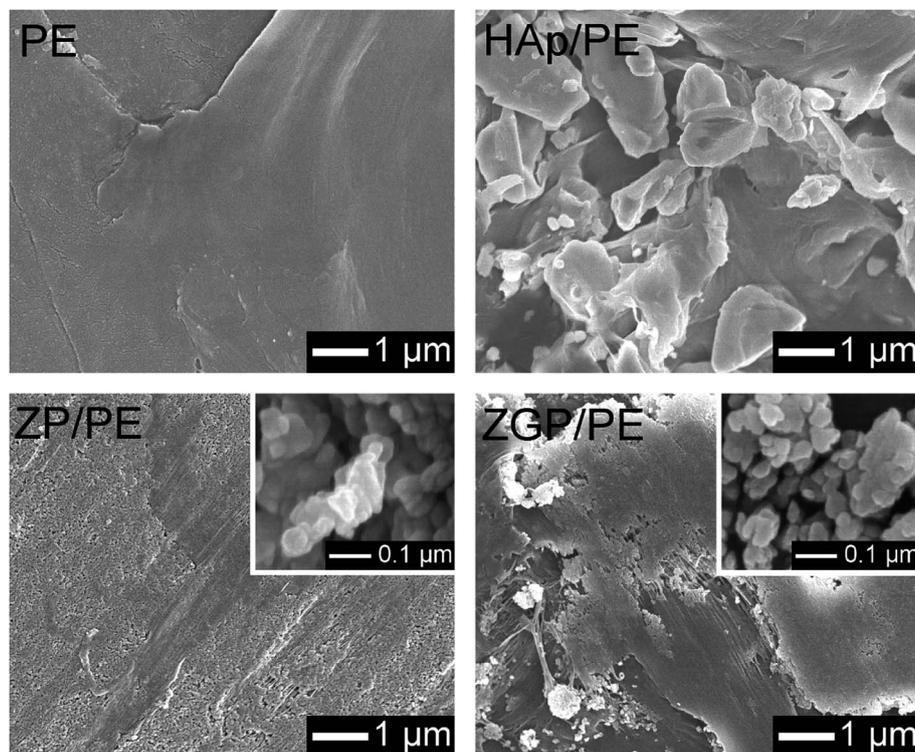

Fig. 5 FE–SEM images of the prepared substrates. Insets shows images of ZP (left bottom), and ZGP (right bottom) particles.

Table 1 Arithmetic average roughness (R_a) and water droplet contact angle of prepared substrates

| Sample code	$R_a/\mu m$	Contact angle/°
PE	0.53	95
HAp/PE	0.70	105
ZP/PE	0.57	89
ZGP/PE	0.49	93

Hence, the aggregated powders of ZP and ZGP on the surfaces of ZP/PE and ZGP/PE form after the coating processes. There were no significant changes of the crystalline structure of the prepared samples during the coating process on PE. The morphologies observed under FE-SEM indicate that coating of the examined powders resulted in similar surfaces. The results of GI-XRD, Raman spectroscopy, and FE-SEM imaging support the premise that the ZP/PE, ZGP/PE, and HAp/PE coatings had similar microstructures to those of ZP, ZGP, and HAp powders.

Table 1 gives the arithmetic average roughness (R_a) and wettability of the substrates coated with ZP, ZGP, or HAp, as well as uncoated PE substrates. The R_a of the substrates increased in the order of ZP/PE $\simeq$ ZGP/PE $\simeq$ PE < HAp/PE. The substrates showed wettability with contact angles ranging from 89° to 105°, in the order of ZP/PE < ZGP/PE $\simeq$ PE < HAp/PE. The higher contact angle (higher hydrophobicity) was attributed to the rough surface comprising HAp powder.

3.3. Cytocompatibility of the substrates

The cytocompatibility of the substrates was evaluated on the basis of the hASC adhesion behaviour. Fig. 6 shows fluorescence microscopy images of the substrates cultured for 1 h and

24 h. The number of hASCs adhered on the substrates was evaluated by counting their nuclei from the fluorescence images, as shown in Fig. 7. Results are indicated as mean value with bars of standard error. Data were analysed with the paired- or unpaired Student's *t*-test as appropriate for the data set. The difference between a pair of data sets was considered as significant when $p < 0.05$. After culturing for 1 h, PE showed the minimum number of adhered cells among the examined substrates. ZP/PE showed no significant difference in
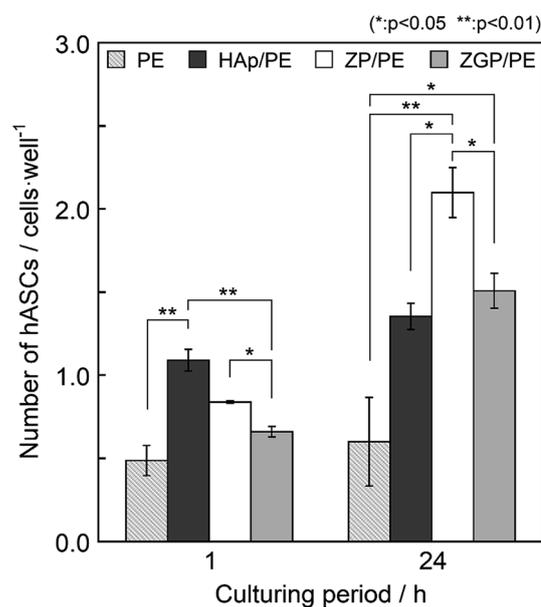
Fig. 7 Number of hASCs adhered on the prepared substrates after being cultured for 1 or 24 h.
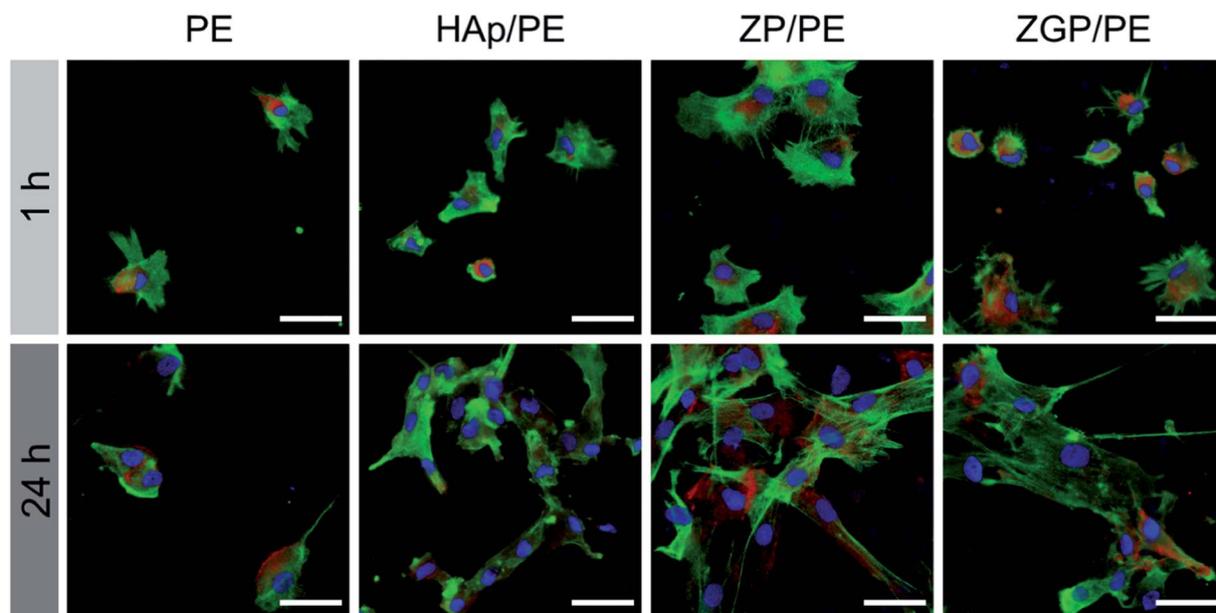
Fig. 6 Fluorescent images of hASCs adhered on the prepared substrates after being cultured for 1 or 24 h. Blue, green, and red fluorescence indicate nucleus, actin cytoskeleton, and vinculin, respectively.
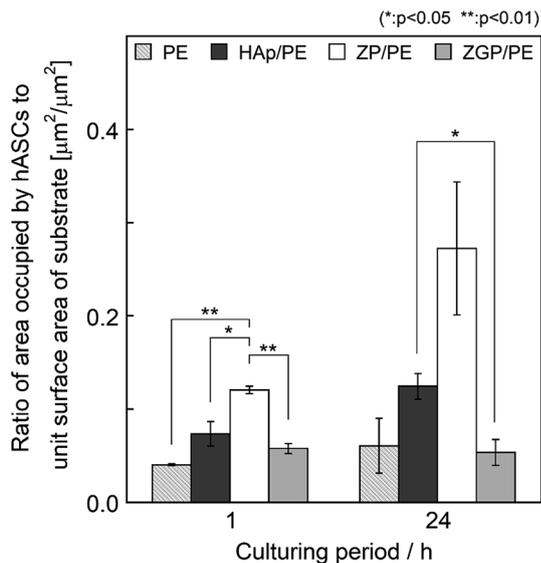
Fig. 8 Ratio of area occupied by hASCs to unit surface area of the prepared substrates after being cultured for 1 or 24 h.

comparison with HAp/PE. After culturing for 24 h, PE maintained the minimum number of the adhered cells among the substrates. ZP/PE and ZGP/PE showed significantly higher numbers of adhered cells than PE, while ZP/PE showed a significantly higher number than HAp/PE. Thus, the ZP/PE and ZGP/PE allowed adhesion of hASCs that is comparable to HAp/PE substrate. Fig. 8 shows the ratio of area occupied by hASCs to unit surface area of the substrate for 1 h and 24 h. Higher coverage area of hASCs means that there is a higher affinity of hASCs to the substrate. ZP/PE showed the highest coverage area among the substrates at both 1 h and 24 h of culturing. The coverage area of ZP/PE were 2.2-times higher than the area of HAp/PE at 24 h of culturing. Hence the α-ZrP had potential to show cytocompatibility comparable to hydroxyapatite. Modification of α-ZrP with β-glycerophosphate suppressed the affinity to hASCs under the present culture condition.

4. Discussion

The layered materials possess a structure wherein hetero-layers with the thickness of a few atoms are stacked *via* weak interactions such as electrostatic forces between counter-charged ions or hydrogen bonding with water molecules. Because of the structural flexibility at the interlayer, organic drug molecules and inorganic ions of various sizes can be inserted between the layers on the basis of the ion-exchanging chemistry.[17,20,31]

The prepared sample of ZP consisted of α-ZrP in crystalline phase with a layered phosphate structure, where the interlayer distance was estimated to be 0.76 nm from the 002 diffraction. Modification of ZP with β-glycerophosphate, lead to expansion of the interlayer distance of 0.85 nm on the diffraction pattern of ZGP. As with the α-ZrP[32] and its organically modified

derivative,[23] the diffraction pattern of ZGP can be indexed as describing a monoclinic lattice with space group $P2_1/c$, which also supports the premise that there is formation of a layered structure in zirconium phosphate compounds. The ZGP was successfully synthesized with an organically modified structure of the interlayer. Generally, α-ZrP has a terminated structure with hydroxy groups on its surface, as indicated by P–OH bonding in the FT-IR spectra. No such group could be detected on ZGP, while P–O–C bonding vibrations were detected. Therefore, the ZGP was modified to be terminated as P–O–$CH(CH_2OH)_2$ (glycerol group). Powder XRD, FT-IR, and Raman spectra of the synthesized ZP and ZGP indicated that water molecules in the α-ZrP disappeared and were replaced by the glycerol group. Although the glycerol group would be 0.41 nm in size, a smaller expansion of 0.10 nm was estimated because of a reduction in the water molecules at the interlayer. Therefore, the hetero-layer of α-ZrP was expected to be covered with glycerol groups. The Raman spectra of both ZP and ZGP showed internal vibration modes (ν_n, $n = 1, 2, 4$) of the PO_4 group and an external vibration mode (R') involving both Zr atoms and PO_4 groups. Therefore, ZGP also has a hetero-layer similar to the structure in α-ZrP. All the evidence supports the formation of α-ZrP modified with β-glycerophosphate. Consequently, organically modified α-ZrP was successfully synthesized after the reflux processing of α-ZrP in a solution containing β-glycerophosphate. ZP/PE showed the minimum contact angle of water among the substrates. This property is contributed to more by the existence of ZP particles on the substrate, while the surface roughness of the substrates coated with various powders appeared to contribute to a lower extent, although the hydrophobicity would be dependent on the roughness of the coated substrates. The highest hydrophilicity was obtained on the ZP/PE substrate, which would be expected to contribute to a high affinity to bone tissues.

Cytocompatibility on ZP/PE was higher than that on HAp/PE, because of significantly wider occupation area after 1 h as well as a significantly larger number of adhered hASCs after 24 h culturing. Lower cytotoxicity of the ZP/PE has been verified *via* proliferation and adhesion of the hASCs, although the initial adhesion of hASCs was lower than that of HAp/PE. The high affinity of α-ZrP is attributed to its structural characteristics. α-ZrP possesses a structure wherein Zr atoms lie in a plane, and the PO_4 groups are alternately placed above and below to form a hetero-layer. Three oxygen atoms of every PO_4 group bond to three Zr atoms in the plane. An oxygen atom of the PO_4 group is negatively charged and neutralised by a proton and acts as a Brønsted acid point. The acidic PO_4 groups that present on the surface of the hetero-layer may determine the compatibility with the cells. Consequently, ZP/PE showed increased wettability and give suitable conditions for attachment and proliferation of hASCs. In contrast, ZGP/PE showed a lowered area of spread of hASCs on its surface because of the appearance of incorporated β-glycerophosphate in the α-ZrP structure. The cytocompatibility of the layered compounds is controlled *via* modification of the interlayer by bonding of functional groups with organic phosphonic acid, phosphate ester, *etc.* Consequently, α-ZrP allows for sufficient cytocompatibility against

hASCs but also the control over the functionality against the cells through modification of its layered structure. This characteristic may enable α-ZrP to be a candidate for use in novel biomaterials.

5. Conclusion

Layered zirconium phosphate and its derivative material modified with β-glycerophosphate molecules were successfully prepared through reflux processing. When human adipose-derived stem cells were seeded on the substrates coated with the layered zirconium phosphate, the cells showed 2.2-times higher occupation area as well as 1.6-times larger number of adhered hASCs after 24 h of culturing than those of substrates decorated with hydroxyapatite.

Conflicts of interest

The authors declare no conflicts of interest associated with this work.

Acknowledgements

References

1 L. Hench and J. Wilson, *Science*, 1984, **226**, 630–636.
2 J. A. Jansen, J. P. C. M. van der Waerden and K. de Groot, *J. Biomed. Mater. Res.*, 1991, **25**, 1535–1545.
3 Y. Shin, H. Aoki, N. Yoshiyama, M. Akao and M. Higashikata, *J. Mater. Sci.: Mater. Med.*, 1992, **3**, 219–221.
4 W. Suchanek and M. Yoshimura, *J. Mater. Res.*, 2011, **13**, 94–117.
5 T. Kanzara, H. Walijee, R. Badar Sheikh, A. Lau and R. Temple, *Eur. Arch. Otorhinolaryngol.*, 2019, **276**, 3067–3072.
6 T. Furuzono, M. Ueki, H. Kitamura, K. Oka and E. Imai, *J. Biomed. Mater. Res., Part B*, 2009, **89**, 77–85.
7 J. Raphel, M. Holodniy, S. B. Goodman and S. C. Heilshorn, *Biomaterials*, 2016, **84**, 301–314.
8 J. S. Fernandes, P. Gentile, R. A. Pires, R. L. Reis and P. V. Hatton, *Acta Biomater.*, 2017, **59**, 2–11.
9 C. Mas-Moruno, B. Su and M. J. Dalby, *Adv. Healthcare Mater.*, 2019, **8**, 1801103.
10 J. Ziegler, D. Anger, F. Krummenauer, D. Breitig, S. Fickert and K.-P. Guenther, *J. Biomed. Mater. Res., Part A*, 2008, **86**, 89–97.
11 H. Schliephake, *J. Oral Maxillofac. Surg.*, 2010, **14**, 17–22.
12 T. N. Vo, F. K. Kasper and A. G. Mikos, *Adv. Drug Delivery Rev.*, 2012, **64**, 1292–1309.
13 S. Suliman, Z. Xing, X. Wu, Y. Xue, T. O. Pedersen, Y. Sun, A. P. Døskeland, J. Nickel, T. Waag, H. Lygre, A. Finne-Wistrand, D. Steinmüller-Nethl, A. Krueger and K. Mustafa, *J. Controlled Release*, 2015, **197**, 148–157.
14 A. López-Galindo, C. Viseras and P. Cerezo, *Appl. Clay Sci.*, 2007, **36**, 51–63.
15 J.-H. Yang, J.-H. Lee, H.-J. Ryu, A. A. Elzatahry, Z. A. Alothman and J.-H. Choy, *Appl. Clay Sci.*, 2016, **130**, 20–32.
16 G. Choi, O.-J. Kwon, Y. Oh, C.-O. Yun and J.-H. Choy, *Sci. Rep.*, 2014, **4**, 4430.
17 A. Díaz, V. Saxena, J. González, A. David, B. Casañas, C. Carpenter, J. D. Batteas, J. L. Colón, A. Clearfield and M. Delwar Hussain, *Chem. Commun.*, 2012, **48**, 1754–1756.
18 A. Díaz, M. L. González, R. J. Pérez, A. David, A. Mukherjee, A. Báez, A. Clearfield and J. L. Colón, *Nanoscale*, 2013, **5**, 11456–11463.
19 A. Clearfield and J. A. Stynes, *Journal of Inorganic and Nuclear Chemistry*, 1964, **26**, 117–129.
20 A. Clearfield and J. M. Kalnins, *Journal of Inorganic and Nuclear Chemistry*, 1976, **38**, 849–852.
21 B. M. Mosby, A. Díaz and A. Clearfield, *Dalton Trans.*, 2014, **43**, 10328–10339.
22 L. Sun, W. J. Boo, H.-J. Sue and A. Clearfield, *New J. Chem.*, 2007, **31**, 39–43.
23 D. M. Poojary, C. Bhardwaj and A. Clearfield, *J. Mater. Chem.*, 1995, **5**, 171–174.
24 K. Momma and F. Izumi, *J. Appl. Crystallogr.*, 2011, **44**, 1272–1276.
25 A. O. Rajeh and L. Szirtes, *J. Radioanal. Nucl. Chem.*, 1999, **241**, 83–91.
26 S. E. Horsley, D. V. Nowell and D. T. Stewart, *Spectrochim. Acta, Part A*, 1974, **30**, 535–541.
27 R. C. T. Slade, J. A. Knowles, D. J. Jones and J. Rozière, *Solid State Ionics*, 1997, **96**, 9–19.
28 C. Y. Ortiz-Avila and A. Clearfield, *J. Chem. Soc., Dalton Trans.*, 1989, 1617–1623, DOI: 10.1039/dt9890001617.
29 P. Colomban and A. Novak, *J. Mol. Struct.*, 1989, **198**, 277–295.
30 S. Zou, J. Huang, S. Best and W. Bonfield, *J. Mater. Sci.: Mater. Med.*, 2005, **16**, 1143–1148.
31 A. Clearfield and R. M. Tindwa, *Journal of Inorganic and Nuclear Chemistry*, 1979, **41**, 871–878.
32 A. Clearfield and S. D. Smith, *J. Colloid Interface Sci.*, 1968, **28**, 325–330.